Journal of Renewable Materials

Tech Science Press

DOI: 10.32604/jrm.2021.015076

ARTICLE

Facile Preparation of a Porous Biochar Derived from Waste Crab Shell with High Removal Performance for Diesel

Xiao Han[1], Zhaodi Wu[1], Yi Yang[1], Jian Guo[1], Yaning Wang[2], Lu Cai[3], Wendong Song[4] and Lili Ji[2,*]

[1]College of Food and Medical, Zhejiang Ocean University, Zhoushan, 316022, China

[2]Institute of Innovation & Application, Zhejiang Ocean University, Zhoushan, 316022, China

[3]Donghai Science and Technology College, Zhejiang Ocean University, Zhoushan, 316000, China

[4]College of Petrochemical and Energy Engineering, Zhejiang Ocean University, Zhoushan, 316022, China

[*]Corresponding Author: Lili Ji. Email: jll-gb@163.com

Received: 19 November 2020 Accepted: 04 January 2021

ABSTRACT

In this study, a porous biochar material derived from waste crab shell was prepared by one-step hydrothermal carbonization and acetic acid activation method at 180°C, which was characterized by SEM, BET, XRD and FTIR. The results show that the as-prepared crab shell biochar (CSB) exhibits a fluffy irregular layered structure with abundant pores and oxygen-containing functional groups, which can facilitate the adsorption of diesel using CSB. In addition, batch adsorption experiments had been performed, effects of initial diesel concentration, adsorption time, adsorbent dosage and pH on the diesel adsorption using CSB were analyzed, which could be observed that CSB has high removal efficiency for diesel, and the maximum removal rate is up to 80.1%. The adsorption isotherms and kinetic studies were also investigated to determine the adsorption mechanism of diesel using CSB, the results show that the Langmuir model and the pseudo-second-order model are more suitable for describing the adsorption of diesel using CSB, indicating that the adsorption of diesel oil by CSB is monolayer chemical adsorption. This study will provide a theoretical basis for the high-value utilization of waste crab shell, which has a great potential in the treatment of oil spill.

KEYWORDS

Waste crab shell; biochar; adsorption; diesel wastewater

1 Introduction

Petroleum, known as the blood of industry, is indispensable to the survival and development of all countries in the world. With the acceleration of industrialization, global petroleum consumption has risen sharply over the last decades, which has reached 4.66 billion metric tons in 2018 [1]. However, at the same time, petroleum and its products could cause environmental pollution in the course of exploitation, refining, storage, transportation and use [2–4], among which, offshore oil spill is one of the main environmental problems that urgently need to be solved in the oil industry. Moreover, oil spills in the natural environment will have disastrous impact on human beings and ecosystems [5,6], and oil contamination usually includes benzene, toluene, ethylbenzene, or petroleum hydrocarbons, which can

enter the human body through the food chain, causing acute and chronic poisoning and damaging the nervous system [7]. Thus, it is imperative for effective removal of oil pollution from the environment.

To date, a variety of technologies available for the removal of oil pollution have been developed, such as physical method [8,9], chemical method [10,11] and biological method [12]. Biological methods have a low remediation rate, which makes them very limited in cleaning up oil spills, while chemical methods can easily cause secondary contamination. In contrast, the physical method has the advantages of simple operation, low cost and quick effect, so it has been drawn considerable attention in recent years, among which, adsorption is the most commonly used physical method. The adsorbent can concentrate the liquid oil and convert it into a semi-solid or solid state to remove it from the polluted solution, so as to avoid the harm to the environment, and at the same time, the adsorbed oil can be recycled [13]. Biochar, as one of the representative absorbents, prepared by high-temperature pyrolysis derived from biomass under low oxygen or oxygen-free condition, has attracted more and more attention, because of its relatively high specific surface area, abundant pore structure and rich functional groups (-OH, C=C, C=O, CH_2 et al.) on its surface [14,15]. In particular, crustacean waste such as crab shells is an abundant and cheap food waste generated by the food processing industry, with an annual production of 1 million tons [16]. Crab shell is a natural porous structure complex [17] composed of protein (20%–40%), chitin (15%–40%) and calcite (20%–50%) [18] and is considered a highly promising candidate for biochar preparation [19]. The preparation of biochar using crab shells can not only reduce the serious environmental pollution caused by various chemicals or microorganisms decomposed from waste crab shells [19,20], but also produce low-cost, renewable and sustainable biochar raw materials. It has been reported that crab shells have been developed into various biochar materials with rich porous structure and high specific surface area, which are used as bio-adsorbent for the removal of organic dyes, heavy metals, and diesel fuel [21–24]. However, almost all biomass carbon based adsorption modified materials in the literature were treated by high temperature pyrolysis followed by activation with potassium hydroxide [25]. This method not only consumes a lot of energy, but also the process is complex, cumbersome, and highly environmentally friendly [26].

Commonly used biochar preparation methods include high-temperature cracking (also known as oxygen-limited carbonization) and hydrothermal carbonization [27]. Compared with the traditional high-temperature pyrolysis carbonization technology, hydrothermal carbonization has obvious advantages such as low energy consumption, high efficiency of carbon element fixation, and carbide surface rich in oxygen-containing and nitrogen-containing functional groups [28], which can be widely used in various fields. It has great potential for application in wasting biomass treatment/pre-treatment and resource utilization [29,30]. As is well known, the quality and property of biochar depend on the characteristics of raw material and activation method [31,32]. At present, activation method contains physical and chemical activation, among which, chemical activation is extensively employed to prepare biochar due to its advantages of high yield, short time and large specific surface [33,34]. Now, the commonly used chemical activators include KOH [35], H_3PO_3 [34], NaOH [36], $ZnCl_2$ [32], etc. However, the above activators still face the challenges of high energy consumption and probably causing corrosion to the instrument. The advantages of using organic acids as activators compared to strong acids, bases and salts are environmental friendliness, low cost and the use of low toxic reactants [37]. It has been successfully used as an effective activator for low-temperature preparation of biochar from different types of raw materials such as soybean straw [38], corn cobs [39] and lawn grass [40].

However, to the best of our knowledge, there are few reports on the preparation of crab shell biochar by hydrothermal carbonization using acetic acid as an activator. In this study, a porous biochar derived from waste crab shell was prepared by one-step hydrothermal carbonization and activation method at low temperature using acetic acid as activation reagent. CSB was characterized by SEM, BET, XRD and FTIR. The adsorption properties of as-prepared biochar for diesel oil were investigated by simulating the

environment of diesel wastewater. The batch adsorption experiments of diesel were performed using as-prepared absorbent, and the adsorption isotherms and kinetics were also investigated.

2 Experimental

2.1 Materials

Crab shell used in this experiment was obtained from the local market in Zhoushan, China, which was washed with deionized water for several times and dried at 80°C for 2 h. Then the dried crab shell was crushed into powder and used in subsequent pyrolysis experiments. Hydrochloric acid (HCl), sodium hydroxide (NaOH) and acetic acid (CH_3COOH) were purchased from Shanghai National Pharmaceutical Chemical Reagent Co., Ltd., China. The chemicals used in this study are analytical and used at reception without further purification.

2.2 Preparation of Crab Shell Biochar

The pre-treated crab shell powder was soaked in 6% HCl for 4 h at 30°C for decalcification, and then soaked in 6% NaOH for 2 h at 90°C for deproteinization. After being soaked in 50% NaOH for 9 h, the crab shell powder was washed with deionized water for several times until neutral (pH = 7), and then dried in the oven (SENXIN-DGG9030BD, Shanghai, China) at 80°C for 10 h. The pretreated crab shell powder mixed was with 50% acetic acid (crab shell/acetic acid (w/v) = 1:1), then the mixture was carbonized at 180°C for 10 h in the oven. After cooling to room temperature, the prepared crab shell biochar was rinsed using deionized water until neutral, dried in the in the oven at 80°C for 12 h, ground and sieved with 100 mesh, which was denoted as CSB. And in the control group, the pretreated crab shell powder in "*2.1 Materials*" was denoted as CS.

2.3 Characterization of Crab Shell Biochar

Surface microstructure and morphology of as-prepared sample were investigated by using scanning electron microscopy (SEM, Hitachi S-4800, Tokyo, Japan) at 5.0 KV. N_2 adsorption/desorption isotherm was performed on a static volumetric adsorption analyzer (Micromeritics ASAP 2010, Shanghai, China) and calculated with the method of BET. Meanwhile, X-ray diffraction (XRD) patterns of sample were recorded on an Ultima IV X-ray Diffractometer (Ultima IV, Rigaku Corporation, Tokyo, Japan) in the range of 2θ from 10° to 60°. Moreover, the surface functional groups were analyzed by Fourier transform infrared spectra (FTIR, Nicolet 5700, Thermo Corp., USA).

2.4 Batch Adsorption Experiments

2.4.1 Determination of Diesel Standard Curve

The standard curve is a curve used to describe the quantitative relationship between the concentration (or content) of the substance to be measured and the response signal values of the analytical instrument. Using the diesel standard solution to draw the diesel standard curve, the corresponding concentration value can be found on the standard curve through the measured absorbance value.

0.3 g diesel was mixed with 5 mL petroleum ether in a 100 mL volumetric flask, diluted with petroleum ether to 100 mL, as the diesel standard solution. Take 0 mL, 5 mL, 10 mL, 15 mL, 20 mL and 25 mL diesel standard solution, respectively, and the constant volume was made up to 25 mL with petroleum ether. The absorbance value was measured with petroleum ether as reference at a wavelength of 256 nm by UV-vis spectrophotometer (Model No. UV 2600, Shimadzu, Shanghai, China), and the diesel standard curve was drawn as shown in Fig. S1.

2.4.2 Batch Adsorption Experiments

The as-prepared absorbent was added into 100 mL diesel wastewater for adsorption experiments. The effects of diesel initial concentration, reaction time, initial pH and absorbent dosage on the diesel

adsorption were also investigated as shown in Tab. 1. The diesel initial concentration was 100 mg/L, 200 mg/L, 300 mg/L, 400 mg/L, 500 mg/L and 600 mg/L, respectively, the reaction time was 0.5 h, 1 h, 2 h, 3 h, 4 h and 6 h, respectively, the initial pH value was adjusted from 5.0–9.0 with 0.1 mol/L HCl or 0.1 mol/L NaOH and the absorbent dosage was 0.05 g, 0.10 g, 0.15 g, 0.20 g and 0.25 g, respectively. After adsorption, the reaction solution was centrifugal in a desktop high-speed centrifuge (Cence, TG16-WS, Hunan, China) at 1700 g for 5 min, and the supernatant was collected to measure its optical density value (UV 2600, Shimadzu, Japan) at 256 nm. The diesel fuel concentration (C_0 and C_e) in diesel wastewater was then calculated from the OD values. The adsorption rate (R) and equilibrium adsorption capacity (q_e) of diesel fuel can be calculated according to Eqs. (1) and (2), respectively.

$$\mathrm{R}(\%) = \frac{C_0 - C_e}{C_0} \times 100\% \tag{1}$$

$$q_e = \frac{(C_0 - C_e)V}{m} \tag{2}$$

where, the adsorption rate of diesel at equilibrium is denoted as R (%), the adsorption capacity of diesel at equilibrium is denoted as qe, the initial and equilibrium concentrations of diesel wastewater are denoted as C0 and Ce, respectively, and the dosage of CSB and the volume of diesel wastewater solution are denoted as m(g) and V(L), respectively.

Table 1: Batch adsorption experimental design

Conditions	Diesel initial concentration (mg/L)	Adsorption time (h)	Adsorption pH	Absorbent dosage (g)
1	100	0.5	5	0.05
2	200	1	6	0.10
3	300	2	7	0.15
4	400	3	8	0.20
5	500	4	9	0.25
6	600	6		

2.5 Adsorption Isotherm and Kinetic Studies

0.1 g CSB absorbent was added into 100 mL diesel wastewater with different initial concentrations, respectively, and the adsorption process was carried out for 5 h. The Langmuir and Freundlich adsorption isotherms were used to analyze the equilibrium performance, as follows:

$$\frac{C_e}{q_e} = \frac{C_e}{q_m} + \frac{1}{K_L q_m} \tag{3}$$

$$q_e = K_F {C_e}^{1/n} \tag{4}$$

where the equilibrium concentration of diesel fuel is denoted as C_e (mg/L). The adsorption capacity of diesel fuel at equilibrium is denoted as q_e (mg/g), and the saturation adsorption capacity is denoted as q_m (mg/g). The Langmuir adsorption equilibrium constant is denoted by K_L (L/mg) and the Freundlich constant is denoted by K_F [(mg/g)(L/mg)1/n], 1/n representing the energy partition depending on the adsorption properties and adsorbent energy.

0.1 g CSB adsorbent was added to 100 mL/L, 300 mg/L and 600 mg/L of 100 mL diesel wastewater and the adsorption capacity of diesel was determined at different adsorption times from 0 to 300 min at 25°C. The adsorption kinetics of the prepared samples were analyzed by proposed primary reaction (PFO) and secondary kinetics (PSO) as follows:

$$\ln(q_e - q_t) = \ln q_e - k_1 t \tag{5}$$

$$\frac{t}{q_t} = \frac{1}{k_2 q_e{}^2} + \frac{t}{q_e} \tag{6}$$

where the amount of diesel adsorbed at adsorption equilibrium and at time t(min) are recorded as q_e(mg/g) and q_t(mg/g), respectively. The rate constants of PFO and PSO are k_1(min^{-1}) and k_2(g/mg min), respectively, and the time is recorded as t(min).

3 Results and Discussion

3.1 Characterization of Crab Shell Biochar

3.1.1 SEM Analysis

SEM is employed to visualize the surface morphology and microstructure of as-prepared samples, as shown in Fig. 1. It could be demonstrated that crab shell exhibits a dense stacked layered structure with a few unevenly distributed grooves in Figs. 1a and 1b. After pyrolysis, CSB shows a fluffy irregular layered structure, including a large number of pores and grooves as indicated in Figs. 1c and 1d (as shown by the red arrow).This is because the chitin derivatives of crab shells acetylation by acid-base treatment of decalcification and deproteinization [41,42] and the activator acetic acid in the process of hydrothermal carbonization of dehydration and decarboxylation, hydrogen bond breakage, free radical reaction breakage [43] and aromatization, condensation and solidification reaction to generate biochar [44,45].The rough surface of crab shell biochar is beneficial to the adsorption of diesel oil, and the loose groove structures are conducive to the adsorption and storage of a large amount of diesel oil [46].

3.1.2 BET Analysis

The N_2 adsorption isotherm and pore size distribution of as-prepared sample was shown in Fig. 2. According to IUPAC classification [47], the N_2 adsorption isotherm of CSB is Type IV, whose bifurcation is irreversible. And there is a hysteresis loop at P/P0 > 0.4 in the adsorption isotherm of CSB, indicating the formation of mesoporous structure. Based on the N_2 adsorption bifurcation data, the pore size distribution (PSD) of CSB is further analyzed by using the non-local density functional theory (NLDFT) model [26]. As shown in the Fig. 2b, CSB shows a relatively sharp PSD, centered around 3 nm–5 nm, and PSD is mainly in the range of 3 nm–20 nm, which consists of micropore and mesopore. In addition, the specific surface area and pore volume of CS obtained from N_2 adsorption isotherm data are 9.57 m^2/g and 0.027 cm^3/g, respectively, while those of CSB are 17.01 m^2/g and 0.0763 cm^3/g, respectively. Compared with CS, the specific surface area of CSB increases by 78%, which was caused by the decarboxylation and dehydration of crab shells during the hydrothermal carbonization process [43]. Some volatile substances such as CO_2, CO and H_2O overflowed from the pores and destroyed the original structure of crab shells, which led to the gradual formation of micropores and the increase in specific surface area and pore volume of biochar.

3.1.3 XRD Analysis

The XRD pattern is utilized to analyze the crystal structure and phase analysis of the as-prepared sample, as shown in Fig. 3. It can be seen from the following X-ray diffraction patterns that the observed diffraction peaks located at crystal planes of $CaCO_3$ according to JCPDS database No. 81-2027 [31]. As for the pattern of CS, the observed diffraction peaks located at about 23°, 29°, 39°, 43°and 48°, can be perfectly indexed to

the (012), (104), (113), (202), (018) of crystal planes of $CaCO_3$, and there is a diffraction peak at about 2θ = 19° corresponding to (21-2) crystal planes of chitin [48]. After pyrolysis, the $CaCO_3$ peaks are weak, only 23° and 39° diffraction peaks left in the XRD pattern of CSB, while the chitin peak located at 19° obviously strengthens. As is well known, chitin is rich in hydroxyl groups, which could provide abundant binding sites for diesel adsorption using crab shell biochar.

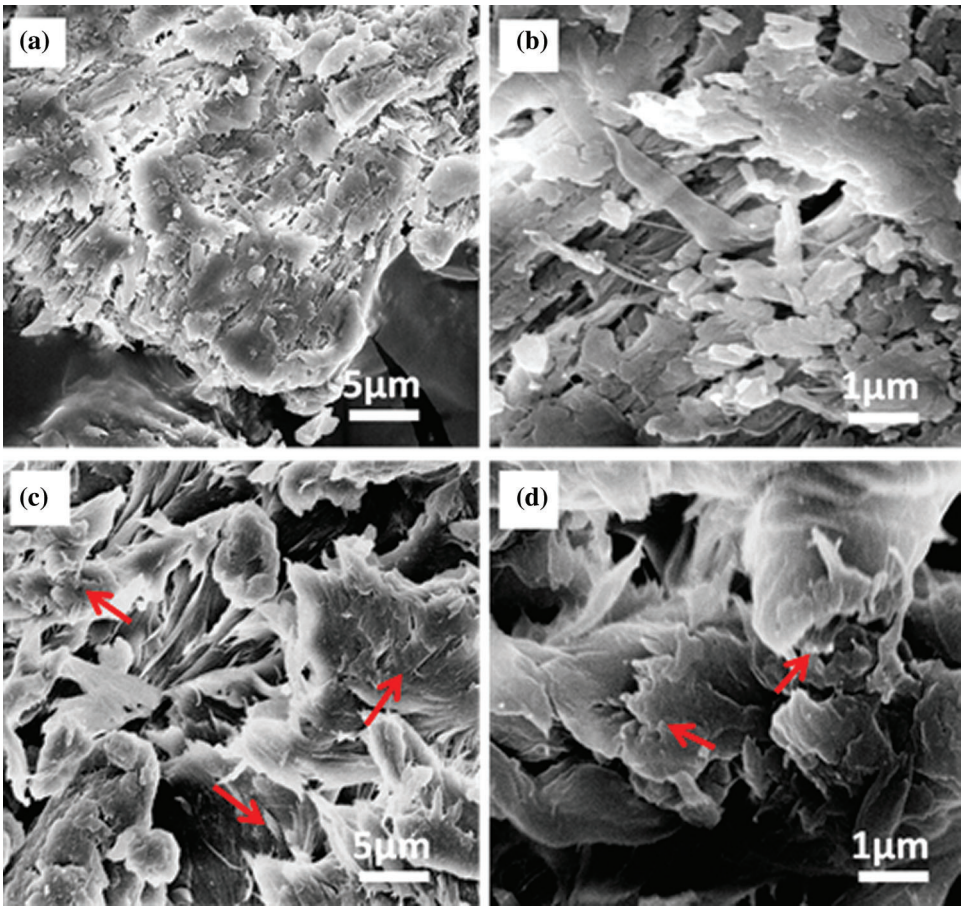

Figure 1: SEM images of CS (a, b) and CSB (c, d)

3.1.4 FTIR Analysis

The surface chemical compositions and surface functional groups of as-prepared samples are analyzed by the FT-IR, as illustrated in Fig. 4. The FTIR spectrums of the CS and CSB located at 3273.2 cm^{-1} and 3259.6 cm^{-1} are attributed to the axial O-H stretching vibration [38], followed by a peak at 2358.9 cm^{-1} due to R-N=C=O stretching vibration. The absorption peak at 1668.4 cm^{-1} in the CS and CSB spectra is attributed to the C=O [49] stretching vibration caused by the carboxyl group (COOH) introduced by acetic acid on the surface of biochar [37]. Furthermore, the adsorption peaks located at 1070.4 cm^{-1} and 1072.4 cm^{-1} in the CS and CSB spectra were attributed to symmetric stretching vibrations of X-H due to amine/ester, followed by peaks located at 871.82 cm^{-1} and 893.04 cm^{-1} due to out-of-plane bending vibrations of C-H.

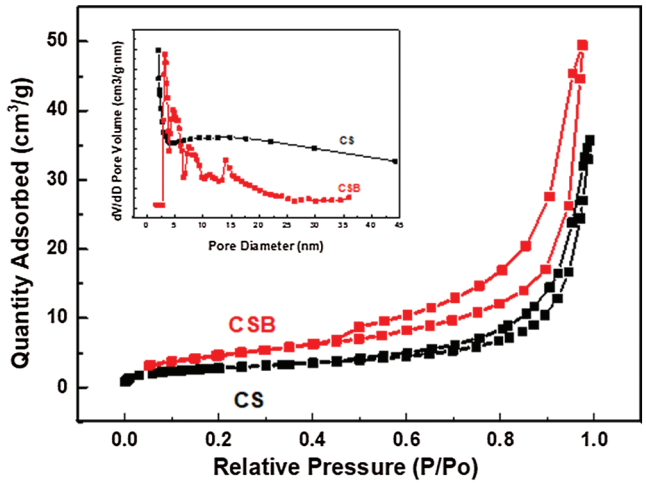

Figure 2: N_2 adsorption-desorption isotherm and pore size distribution of CS and CSB

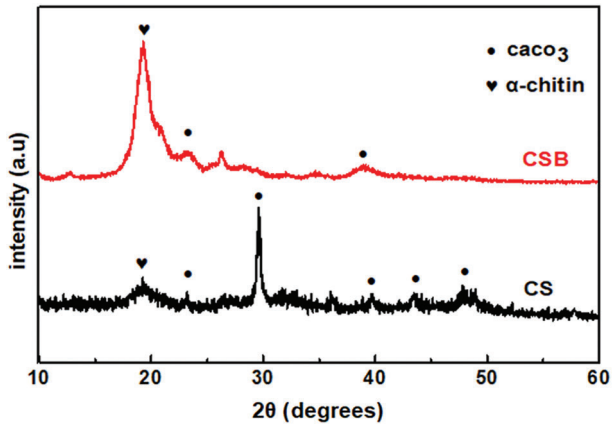

Figure 3: X-ray diffraction patterns of CS and CSB

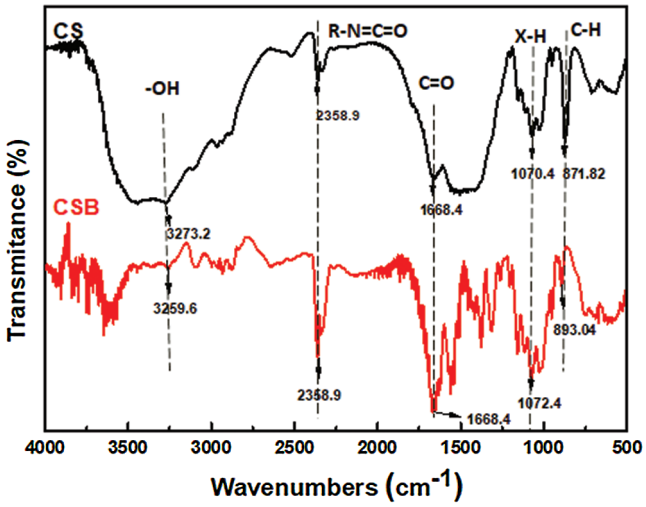

Figure 4: FTIR spectra of crab shell and crab shell biochar

The carboxyl functional group is esterified with the alcohol contained in diesel oil, so it may play a key role in the adsorption of diesel oil [49]. Ester group (R-N=C=O), halogen group (X-H) and alkyl group (C-H) are lipophilic groups that can form van der Waals force between diesel and diesel molecules [50]. The hydroxyl groups enriched in CSB can undergo radical substitution reactions with alkanes in diesel fuel [51]. Therefore, it can be speculated that chemisorption is the main driving force for diesel fuel adsorption using CSB. From the above discussion, it can be seen that the reactive groups on the crab shell surface become enriched after activation and are more favorable for diesel adsorption.

3.2 Batch Adsorption Experiments

3.2.1 Effect of Initial Diesel Concentration

Fig. 5a shows the adsorption performances of CSB to different initial diesel concentrations. It could be demonstrated that the residual concentrations of diesel in the adsorption system decrease sharply in 10 mins, decrease gradually as the adsorption time increase until equilibrium, and reach the adsorption equilibrium at 180 mins. It can be calculated that the adsorption rates of as-prepared sample for diesel wastewater at different initial concentrations are 77.7%, 78.3%,79%, 79.5%, 79.7% and 80.1%, respectively, that is the higher the initial concentration of diesel, the greater the adsorption capacity of diesel using CSB. At the beginning of the adsorption time, the high removal rate of diesel using CSB is due to at the initial stage of adsorption, the functional groups on the surface of biochar and the internal pores are well developed and diesel particles can easily adhere to them, and then because the outer surface of the adsorbent is occupied by oil, the oil removal rate decreases and reaches equilibrium [52]. With the increase of diesel solution concentration, the time to reach equilibrium becomes longer, which is because more active sites are occupied, resulting in competitive adsorption, and decreasing the attractiveness of CSB to diesel [53].

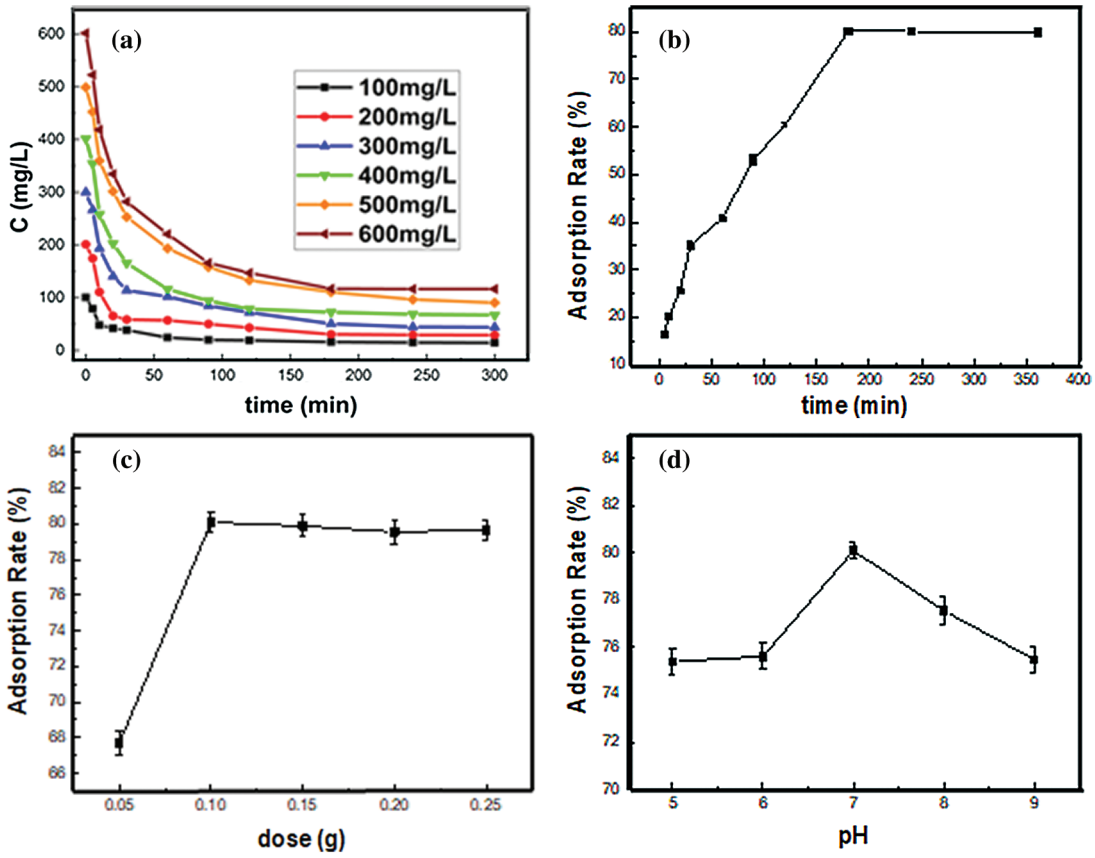

Figure 5: Effects of initial diesel concentration (a), adsorption time (b), dosage (c) and pH (d) on the adsorption of diesel by CSB

3.2.2 Effect of Adsorption Time

Fig. 5b shows the effect of adsorption time on the adsorption capacity of diesel using CSB. It can be observed that the diesel adsorption rate first increases rapidly until adsorption equilibrium at 180 min, and the maximum diesel adsorption rate is 80.1%. Initially, the higher adsorption efficiency is due to abundant binding sites available on the surface of CSB, which could enhance the adsorption of diesel. In addition, low solubility and higher hydrophobicity of diesel are beneficial to providing more attraction towards CSB, rendering high adsorption efficiency for diesel using CSB. At adsorption equilibrium stage, the binding sites of CSB have been covered with diesel, and the amount of diesel in solution and the amount of diesel adsorbed on CSB are in dynamic equilibrium [54].

3.2.3 Effect of Adsorbent Dosage

The adsorption capacities of CSB dose for diesel are shown in Fig. 5c. It can be seen that with increasing CSB dose in the range of 0.05 g–0.25 g, the adsorption capacities of CSB for diesel sharply increase and then gradually flatten. That is because there are more binding sites with the increase of CSB, being beneficial to adsorb more diesel, while CSB dose increases to 0.1 g, adsorption system reaches equilibrium, and the adsorption of diesel using CSB tends to be stable.

With the increase of the amount of CSB, its binding sites and adsorption capacity will be increased, however, after reaching its peak, the adsorption capacity of CSB would reach saturation, and the adsorption rate will not be further improved. Moreover, too much biochar will make them adhere together in solution, which will also reduce its specific surface areas, the adsorption sites will also be reduced, so that the adsorption rate will even slightly decrease [55].

3.2.4 Effect of pH

Fig. 5d shows the effect of pH in diesel adsorption using CSB in the range of 5 to 9. The adsorption performance of diesel using CSB is favored at pH = 7, where the maximum absorption rate is 70%. This is because under acidic conditions, H^+ neutralizes the negative charge on the surface of oil molecules, and the stability is broken, resulting in the condensation of oil droplets [56]. However, with the increase of pH value, the viscosity of diesel decreases by the reaction of organic acids or acidic components in diesel with OH^- in solution, and the diesel molecules are easily desorbed and dispersed [57]. Therefore, it can be concluded that electrostatic interaction would be one of the main factors that influence the adsorption capacity of diesel using CSB.

3.3 Adsorption Isotherm and Kinetic Studies

3.3.1 Adsorption Isotherm Studies

In order to study the adsorption equilibrium, Langmuir and Freundlich adsorption isotherm models were employed to evaluate the equilibrium characteristics. Fig. 6 indicates the fitting of data with these two isotherm models, and Tab. 2 shows the adsorption parameters and regression data of the models. The R^2 value of the Langmuir isotherm is 0.996, and that of the Freundlich isotherm is 0.968, thus the Langmuir equation is more suitable for describing the adsorption of diesel using CSB, being used to calculate the adsorption amount of diesel using CSB at equilibrium is 451 mg/g at 25°C, in good combination with experimental data (480.6 mg/g). Thus, it could be demonstrated that the adsorption of diesel using CSB is monolayer surface adsorption [37].

3.3.2 Adsorption Kinetics Studies

To investigate the kinetic mechanism of diesel adsorption using CSB, kinetic models were fitted to diesel adsorption data at 100, 300 and 600 mg/L diesel concentrations using pseudo-first order (PFO) model and pseudo-second order (PSO) model. Fig. 7 shows the fit of experimental data to the kinetic model using CSB for diesel fuel, and Tab. 3 shows the results of the kinetic model fit for diesel fuel adsorption using

CSB. It can be seen that comparing the R^2 values of PSO model and PFO model with three diesel concentrations. The R^2 value of PSO model is higher. Therefore, the PSO model is more suitable for describing the adsorption process of CSB on diesel fuel and is used to calculate the adsorption amount of diesel fuel at equilibrium (89.45 mg/g, 258.24 mg/g and 486.32 mg/g) which fits well with the experimental data (77.7 mg/g, 237 mg/g and 480.6 mg/g). It can be possible to conclude that the adsorption of CSB on diesel is a chemisorption, which may involve the electron exchange between the functional groups on the surface of CSB and diesel molecules [58,59].

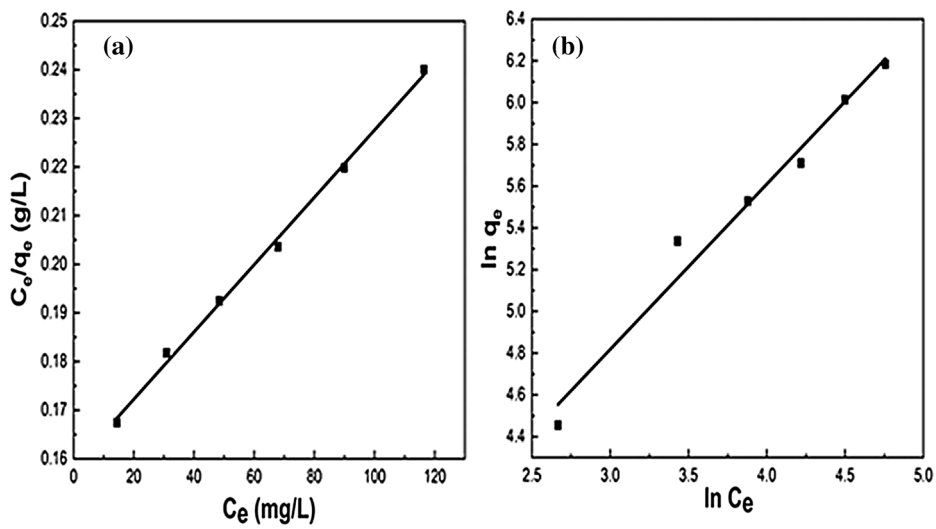

Figure 6: The adsorption isotherm models of diesel using CSB plotted with (a) the Langmuir equation and (b) the Freundlich equation

Table 2: The adsorption isotherm parameters for diesel adsorption using CSB

	Langmuir			Freundlich		
Temperature (°C)	q_L(mg/g)	K_L(L/g)	R^2	n	K_F(L/g)	R^2
25	451	0.679	0.996	1.263	11.48	0.968

3.3.3 Comparison with Other Adsorbents

Tab. 4 shows the comparison of the maximum adsorption capacities of different adsorbents for diesel. It is observed from the results that CSB has relatively higher adsorption capacity (480.6 mg/g) compared with other adsorbents previously reported in literature. The high adsorption rate of diesel on CSB can be attributed to abundant active sites available and high surface area of CSB, which could adsorb diesel molecules effectively. Furthermore, crab shell as by-product of seafood products, could be easily obtained with low cost and can realize the value-added utilization of waste. Thus, crab shell biochar has great potential for the treatment of oil spill.

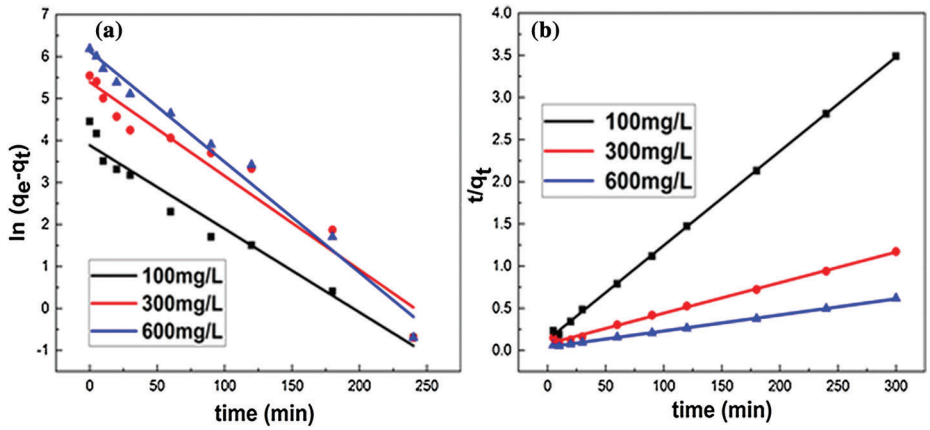

Figure 7: Adsorption Kinetics of diesel adsorbed by CSB, (a) pseudo first order model; (b) pseudo second order model

Table 3: The adsorption kinetic parameters of diesel using CSB

Kinetic model	Parameters	Values		
		100 mg/L	300 mg/L	600 mg/L
Pseudo-first-order	q_e(mg/g)	48.77	220.06	457.86
	k_1(min^{-1})	0.019	0.022	0.026
	R^2	0.959	0.941	0.981
Pseudo-second-order	q_e(mg/g)	89.45	258.24	486.32
	k_2(g/mg min) × 10^{-3}	0.991	0.227	0.107
	R^2	0.999	0.995	0.998
CSB adsorption capacity	q_e(mg/g)	77.7	237	480.6

Table 4: Comparison of adsorption capacity of different adsorbents for diesel removal

Adsorbent	qmax (mg/g)	Experimental conditions			Reference
		Adsorbent dose	pH	Time	
Crab shell biochar modified by potassium hydroxide	93.9	0.2 g	7	240 min	[24]
Corn husk	430	10 mg/L	7–8	60 min	[60]
Sepiolite modified by tetradecyl trimethyl ammonium bromide (TTAB-Sep)	434.7	7 g/L	6	240 min	[61]
Sepiolite	190	10 g	6.7	1440 min	[62]
CSB	480.6	0.1 g	7	180 min	This work

4 Conclusions

In sum, a novel carb shell biochar was prepared by a one-step hydrothermal carbonization and activation method, in which, acetic acid chosen as activator could achieve low-temperature activation. It can be

observed from SEM, BET, XRD and FT-IR characterizations that the as-prepared sample is a fluffy irregular layered structure with abundant pores and oxygen-containing functional groups, being beneficial to the adsorption of diesel using CSB. Moreover, the batch adsorption experiments indicate that CSB has high adsorption performances for diesel, and the maximum removal rate is up to 80.1%. And the Langmuir model and the pseudo-second-order model could better describe the adsorption process of diesel using CSB.

Funding Statement: This study was supported by the Fundamental Research Funds for Zhejiang Provincial Universities and Research Institutes (Nos. 2019J00045, 2019J00025), the General Research Project of Zhejiang Province Education Department (No. Y202044721) and Key Research and Development Projects of Zhejiang Province of China (No. 2018C02043).

Conflicts of Interest: The authors declare that they have no conflicts of interest to report regarding the present study.

References

1. Wang, T. (2019). Global oil consumption from 1970 to 2018. *Chemicals and Resources, 9*. https://www.statista.com/statistics/265261/global-oil-consumption-in-million-metric-tons/.
2. Drevon, C. A. (1992). Marine oils and their effects. *Nutrition Reviews, 50(4),* 38–45. DOI 10.1111/j.1753-4887.1992.tb01288.x.
3. Jackson, J. B. C., Cubit, J. D., Keller, B. D., Batista, V., Burns, K. et al. (1989). Ecological effects of a major oil spill on Panamanian coastal marine communities. *Science, 243(4887),* 37–44. DOI 10.1126/science.243.4887.37.
4. Jernelöv, A. (2010). How to defend against future oil spills. *Nature, 466(7303),* 182–183. DOI 10.1038/466182a.
5. Zhu, H., Qiu, S., Jiang, W., Wu, D. X., Zhang, C. Y. (2011). Evaluation of electrospun polyvinyl chloride/polystyrene fibers as sorbent materials for oil spill cleanup. *Environmental Science & Technology, 45 (10),* 4527–4531. DOI 10.1021/es2002343.
6. Ilker, Y. T., Gulsah, O. A., Hayal, B. S. (2016). Cross-linked poly (tetrahydrofuran) as promising sorbent for organic solvent/oil spill. *Journal of Hazardous Materials, 309,* 210–218. DOI 10.1016/j.jhazmat.2016.02.014.
7. Solomon, G., Janssen, S. (2010). Health effects of the Gulf oil spill. *JAMA, 304(10),* 1118–1119. DOI 10.1001/jama.2010.1254.
8. Victoria, B., Arturo, A. K. (2006). Improved mechanical oil spill recovery using an optimized geometry for the skimmer surface. *Environmental Science & Technology, 40(24),* 7914–7918. DOI 10.1021/es061842m.
9. Crick, C. R., Bhachu, D. S., Parkin, I. P. (2014). Superhydrophobic silica wool—A facile route to separating oil and hydrophobic solvents from water. *Science and Technology of Advanced Materials, 15(6),* 065003. DOI 10.1088/1468-6996/15/6/065003.
10. Mullin, J. V., Champ, M. A. (2003). Introduction/overview to *in situ* burning of oil spills. *Spill Science & Technology Bulletin, 8(4),* 323–330. DOI 10.1016/S1353-2561(03)00076-8.
11. Rosales, P. I., Suidan, M. T., Venosa, A. D. (2010). A laboratory screening study on the use of solidifiers as a response tool to remove crude oil slicks on seawater. *Chemosphere, 80(4),* 389–395. DOI 10.1016/j.chemosphere.2010.04.036.
12. Crisafi, F., Genovese, M., Smedile, F., Russo, D., Catalfamo, M. et al. (2016). Bioremediation technologies for polluted seawater sampled after an oil-spill in Taranto Gulf (Italy): A comparison of biostimulation, bioaugmentation and use of a washing agent in microcosm studies. *Marine Pollution Bulletin, 106(1−2),* 119–126. DOI 10.1016/j.marpolbul.2016.03.017.
13. Wu, D. X., Fang, L. L., Qin, Y. M., Wu, W. J., Mao, C. M. et al. (2014). Oil sorbents with high sorption capacity, oil/water selectivity and reusability for oil spill cleanup. *Marine Pollution Bulletin, 84(1–2),* 263–267. DOI 10.1016/j.marpolbul.2014.05.005.
14. Liu, W. J., Jiang, H., Yu, H. Q. (2015). Development of biochar-based functional materials: Toward a sustainable platform carbon material. *Chemical Reviews, 115(22),* 12251–12285. DOI 10.1021/acs.chemrev.5b00195.

15. Zhou, Y. M., Gao, B., Zimmerman, A. R., Chen, H., Zhang, M. et al. (2014). Biochar-supported zerovalent iron for removal of various contaminants from aqueous solutions. *Bioresource Technology, 152,* 538–542. DOI 10.1016/j.biortech.2013.11.021.
16. Lu, S., Gibb, S. W., Cochrane, E. (2007). Effective removal of zinc ions from aqueous solutions using crab carapace biosorbent. *Journal of Hazardous Materials, 149(1),* 208–217. DOI 10.1016/j.jhazmat.2007.03.070.
17. Tian, W. Q., Gao, Q. M., Zhang, L. M., Yang, C. X., Li, Z. Y. et al. (2016). Renewable graphene-like nitrogen-doped carbon nanosheets as supercapacitor electrodes with integrated high energy–power properties. *Journal of Materials Chemistry A, 4(22),* 8690–8699. DOI 10.1039/C6TA02828D.
18. Yan, N., Chen, X. (2015). Sustainability: Don't waste seafood waste. *Nature News, 524(7564),* 155–157. DOI 10.1038/524155a.
19. Ramdani, N., Wang, J., He, X. (2014). Effect of crab shell particles on the thermomechanical and thermal properties of polybenzoxazine matrix. *Materials & Design, 61,* 1–7. DOI 10.1016/j.matdes.2014.04.058.
20. Vijayaraghavan, K., Winnie, H. Y. N., Balasubramanian, R. (2011). Biosorption characteristics of crab shell particles for the removal of manganese(II) and zinc(II) from aqueous solutions. *Desalination, 266(1–3),* 195–200. DOI 10.1016/j.desal.2010.08.026.
21. Dai, L. C., Zhu, W. K., He, L., Tan, F. R., Zhu, N. et al. (2018). Calcium-rich biochar from crab shell: An unexpected super adsorbent for dye removal. *Bioresource Technology, 267,* 510–516. DOI 10.1016/j.biortech.2018.07.090.
22. Samia, R., Julian, D., Marc, S. (2019). A The potential use of natural vs commercial biosorbent material to remediate stream waters by removing heavy metal contaminants. *Journal of Environmental Management, 231,* 275–281.
23. Dai, L. C., Tang, F. R., Li, H., Zhu, N. M., He, M. X. et al. (2017). Calcium-rich biochar from the pyrolysis of crab shell for phosphorus removal. *Journal of Environmental Management, 198,* 70–74. DOI 10.1016/j.jenvman.2017.04.057.
24. Cai, L., Zhang, Y., Zhou, Y., Zhang, X., Ji, L. et al. (2019). Effective adsorption of diesel oil by crab-shell-derived biochar nanomaterials. *Materials, 12(2),* 236. DOI 10.3390/ma12020236.
25. Wang, Y., Liu, R. (2017). Comparison of characteristics of twenty-one types of biochar and their ability to remove multi-heavy metals and methylene blue in solution. *Fuel Processing Technology, 160,* 55–63. DOI 10.1016/j.fuproc.2017.02.019.
26. Chen, B. L., Yang, Z. X., Ma, G. P., Kong, D. L., Xiong, W. et al. (2018). Heteroatom-doped porous carbons with enhanced carbon dioxide uptake and excellent methylene blue adsorption capacities. *Microporous and Mesoporous Materials, 257,* 1–8.
27. Tekin, K., Karagöz, S., Bektaş, S. (2014). A review of hydrothermal biomass processing. *Renewable and Sustainable Energy Reviews, 40,* 673–687.
28. Jian, X. M., Zhuang, X. Z., Li, B. S., Xu, X. W., Wei, Z. B. et al. (2018). Comparison of characterization and adsorption of biochars produced from hydrothermal carbonization and pyrolysis. *Environmental Technology & Innovation, 10,* 27–35.
29. Liu, Z. G., Quek, A., Hoekman, S. K., Balasubramanian, R. (2013). Production of solid biochar fuel from waste biomass by hydrothermal carbonization. *Fuel, 103,* 943–949.
30. Judy, A. L., Kyoung, S. R., Claudia, K., Axel, F., Nicole, D. B. et al. (2011). Hydrothermal carbonization of biomass residuals: A comparative review of the chemistry, processes and applications of wet and dry pyrolysis. *Biofuels, 2(1),* 89–124.
31. Yahya, M. A., Al-Qodah, Z., Ngah, C. W. Z. (2015). Agricultural bio-waste materials as potential sustainable precursors used for activated carbon production: A review. *Renewable and Sustainable Energy Reviews, 46,* 218–235.
32. Demiral, H., Demiral, I., Tümsek, F., Karabacakoglu, B. (2008). Pore structure of activated carbon prepared from hazelnut bagasse by chemical activation. *Surface and Interface Analysis, 40(3–4),* 616–619.
33. Nor, N. M., Lau, L. C., Lee, K. T., Abdul, R. M. (2013). Synthesis of activated carbon from lignocellulosic biomass and its applications in air pollution control—A review. *Journal of Environmental Chemical Engineering, 1(4),* 658–666.

34. Martín-González, M. A., González-Díaz, O., Susial, P., Arana, J., Herrera, J. A. et al. (2014). Reuse of Phoenix canariensis palm frond mulch as biosorbent and as precursor of activated carbons for the adsorption of Imazalil in aqueous phase. *Chemical Engineering Journal, 245,* 348–358.
35. Wang, J. C., Senkovska, I., Kaskel, S., Liu, Q. (2014). Chemically activated fungi-based porous carbons for hydrogen storage. *Carbon, 75,* 372–380.
36. Islam, M. A., Tan, I. A. W., Benhouria, A., Asif, M., Hameed, B. H. (2015). Mesoporous and adsorptive properties of palm date seed activated carbon prepared via sequential hydrothermal carbonization and sodium hydroxide activation. *Chemical Engineering Journal, 270,* 187–195.
37. Chen, D. M., Sun, L., Wang, S. G., Yu, Z. B. (2015). Performance, kinetics, and equilibrium of methylene blue adsorption on biochar derived from eucalyptus saw dust modified with citric, tartaric, and acetic acids. *Bioresource Technology, 198,* 300–308.
38. Zhu, B., Fan, T. X., Zhang, D. (2008). Adsorption of copper ions from aqueous solution by citric acid modified soybean straw. *Journal of Hazardous Materials, 153(1–2),* 300–308.
39. Ramos, R. L., Jacome, L. A. B., Rodriguez, I. A. (2005). Adsorption of cadmium(II) from aqueous solution on natural and oxidized corncob. *Separation & Purification Technology, 45(1),* 41–49.
40. Chen, L. H., Ramadan, A., Lv, L. L., Shao, W. J. (2011). Biosorption of methylene blue from aqueous solution using lawny grass modified with citric acid. *Journal of Chemical & Engineering Data, 56(8),* 3392–3399.
41. Younes, I., Rinaudo, M. (2015). Chitin and chitosan preparation from marine sources. Structure, properties and applications. *Marine Drugs, 13,* 1133–1174.
42. Lodhi, G., Kim, Y. S., Hwang, J. W. (2017). Chitooligosaccharide and its derivatives: Preparation and biological applications. *BioMed Research International, 2014,* 654913.
43. Yao, Z. L., Ma, X. Q. (2019). Hydrothermal carbonization of Chinese fan palm. *Bioresource Technology, 282,* 28–36.
44. He, C., Tang, C. Y., Li, C. H., Yuan, J. H., Tran, K. Q. et al. (2018). Wet torrefaction of biomass for high quality solid fuel production: A review. *Renewable & Sustainable Energy Reviews, 91,* 259–271.
45. Kumar, M., Olajire, A. O., Kumar, A. (2018). A review on the current status of various hydrothermal technologies on biomass feedstock. *Renewable and Sustainable Energy Reviews, 81,* 1742–1770.
46. Spagnoli, A. A., Giannakoudakis, D. A., Bashkova, S. (2017). Adsorption of methylene blue on cashew nut shell based carbons activated with zinc chloride: The role of surface and structural parameters. *Journal of Molecular Liquids, 229,* 465–471.
47. Sing, K. S. (1985). Reporting physisorption data for gas/solid systems with special reference to the determination of surface area and porosity (Recommendations 1984). *Pure and Applied Chemistry, 57(4),* 603–619. DOI 10.1351/pac198557040603.
48. Kaya, M., Baran, T., Mentes, A., Asaroglu, M., Sezen, G. et al. (2014). Extraction and characterization of α-chitin and chitosan from six different aquatic invertebrates. *Food Biophysics, 9(2),* 145–157.
49. Wu, M. N., Maity, J. P., Bundschuh, J., Li, C. F., Lee, C. R. et al. (2017). Green technological approach to synthesis hydrophobic stable crystalline calcite particles with one-pot synthesis for oil–water separation during oil spill cleanup. *Water Research, 123,* 332–344. DOI 10.1016/j.watres.2017.06.040.
50. Praveen, P., Loh, K. C. (2013). Trioctylphosphine oxide-impregnated hollow fiber membranes for removal of phenol from wastewater. *Journal of Membrane Science, 437,* 1–6. DOI 10.1016/j.memsci.2013.02.057.
51. Greiner, N. R. (1970). Hydroxyl radical kinetics by kinetic spectroscopy. VII. Reactions with alkanes in the range 300–500°K. *Journal of Chemical Physics, 53(3),* 1284–1285. DOI 10.1063/1.1674133.
52. Hosny, R., Fathy, M., Ramzi, M., Ramzi, M., Moghny, T. A. et al. (2016). Treatment of the oily produced water (OPW) using coagulant mixtures. *Egyptian Journal of Petroleum, 25(3),* 391–396.
53. Gupta, V. K., Jain, R., Siddiqui, M. N., Saleh, T. A., Agarwal, S. et al. (2010). Equilibrium and thermodynamic studies on the adsorption of the dye rhodamine-b onto mustard cake and activated carbon. *Journal of Chemical & Engineering Data, 55(11),* 5225–5229. DOI 10.1021/je1007857.
54. Inbaraj, B. S., Chiu, C. P., Ho, G. H., Yang, J., Chen, B. H. (2006). Chen removal of cationic dyes from aqueous solution using an anionic poly-γ-glutamic acid-based adsorbent. *Journal of Hazardous Materials, 137(1),* 226.

55. Vaghetti, J. C. P., Lima, E. C., Royer, B., Cunha, B. M., Cardoso, N. F. et al. (2009). Pecan nutshell as biosorbent to remove Cu(II), Mn(II) and Pb(II) from aqueous solutions. *Journal of Hazardous Materials, 162(1),* 270–280. DOI 10.1016/j.jhazmat.2008.05.039.
56. Ahmad, A. L., Sumathi, S., Hameed, B. H. (2005). Adsorption of residue oil from palm oil mill effluent using powder and flake chitosan: Equilibrium and kinetic studies. *Water Research, 39(12),* 2483–2494. DOI 10.1016/j.watres.2005.03.035.
57. Zhang, B., Dong, Z. H., Sun, D. J., Wu, T., Li, Y. J. (2017). Enhanced adsorption capacity of dyes by surfactant-modified layered double hydroxides from aqueous solution. *Journal of Industrial and Engineering Chemistry, 49,* 208–218. DOI 10.1016/j.jiec.2017.01.029.
58. Chen, Y. F., Ji, Z., Lin, H., Dong, Y. B. (2014). Removal mechanism of emulsified oil in wastewater by biologic materials modified with lauric acid. *CIESC Journal, 65(6),* 2276–2284.
59. Yang, S., Wang, F., Tang, Q. G., Wang, P. F., Xu, Z. S. et al. (2019). Utilization of ultra-light carbon foams for the purification of emulsified oil wastewater and their adsorption kinetics. *Chemical Physics, 516,* 139–146. DOI 10.1016/j.chemphys.2018.08.051.
60. Augusta, P., Kalaichelvi, P. (2016). Study on removal of emulsified oil from coolant wastewater using corn husk. *Journal of Molecular Liauids, 223,* 1256–1263.
61. Li, Y. F., Wang, M. X., Sun, D. J., Li, Y. L., Wu, T. (2018). Effective removal of emulsified oil from oily wastewater using surfactant-modified sepiolite. *Applied Clay Science, 157,* 227–236. DOI 10.1016/j.clay.2018.02.014.
62. Rajakovic, V., Aleksic, G., Radetic, M., Rajakovic, L. J. (2007). Efficiency of oil removal from real wastewater with different sorbent materials. *Journal of Hazardous Materials, 143(1–2),* 494–499. DOI 10.1016/j.jhazmat.2006.09.060.

Appendix

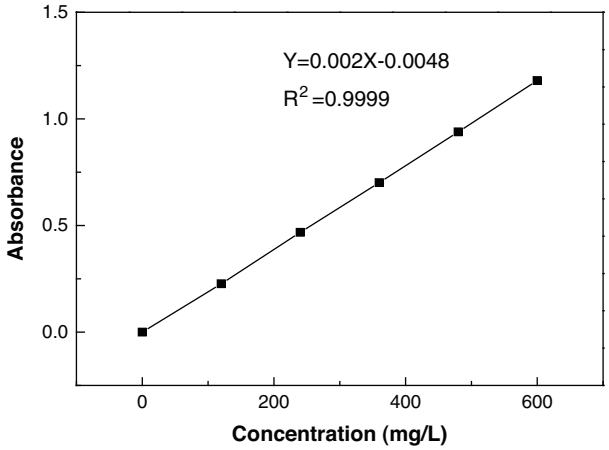

Figure S1: Standard curve of diesel